Transition Metal Chemistry (2019) 44:445–454
https://doi.org/10.1007/s11243-019-00323-5

Two coordination polymers based on mixed 1,4-bis(benzimidazo-1-yl) benzene and O-donor linker ligands: syntheses, crystal structures and properties

Zhuo-Ling Chen[1] · Youzhen Dong[1] · Qing-Wen Liu[1] · Rong-Rong Bian[1] · Wei-Wei Cheng[2] · Yun-Shan Xue[1] · Mei-Pin Liu[3]

Received: 27 January 2019 / Accepted: 4 April 2019 / Published online: 16 April 2019
© Springer Nature Switzerland AG 2019

Abstract

Two coordination polymers based on 1,4-bis(benzimidazo-1-ly)benzene (**L**) and O-donor linking co-ligands, namely $\{[ZnL(mipa)(H_2O)]\}_n$ (**1**) and $\{[Cd_2L_2(sdba)Cl_2]\}_n$ (**2**) (H_2mipa = 5-methylisophthalic acid, H_2sdba = 4,4′-sulfonyldibenzoic acid), have been synthesized under solvothermal conditions and structurally characterized by X-ray single-crystal diffraction. Compound **1** has a 1D chain structure, forming 2D layers by hydrogen bonds. Adjacent layers stack over each other in an ABCD manner along the *c*-axis to further pack into a 3D supramolecular structure supported by π–π interactions. Compound **2** possesses an intriguing 3D architecture, which is constructed from dinuclear $[Cd_2L_4Cl_2]$ secondary building units and V-shaped $sdba^{2-}$ linkers. Both compounds show strong photoluminescence at room temperature with peaks at 362 and 356 nm, respectively, assigned to intraligand and/or ligand-to-ligand charge transfer transitions. Compound **2** can be used as a highly selective probe for Hg^{2+} detection in aqueous solution based on luminescence quenching. The activity of compound **2** as a photocatalyst for the degradation of methylene blue under UV irradiation has been explored.

Introduction

Coordination polymers (CPs) as a relatively new class of crystalline materials have drawn considerable interest, due to their potential applications in a wide variety of fields including catalysis [1–3], luminescent materials [4–6], gas storage and separation [7–9], magnetism [10] and photocatalytic materials [11]. Compared with the more traditional zeolites, the pores and surfaces of CPs possess tunable functionally active sites, such as Lewis acidic/basic sites and open metal sites, which can be adjusted by modification of the organic ligands and judicious choice of metal centers. In order to construct such materials, the design and synthesis of organic linkers with appropriate functional groups are an important consideration. Among numerous available ligands, five-membered N-donor heterocycles (e.g., imidazole, tetrazole, triazole) and their derivatives have attracted extensive attention [12–14]. In this work, we chose a typical N-donor heterocyclic ligand (1,4-bis(benzimidazo-1-ly) benzene) as a basis for the construction of functional coordination polymers, based on the following considerations. First, this ligand usually exhibits simple bridging modes, which should simplify the range of structures of its complexes. Second, such ligands may have good photoluminescent properties, owing to the conjugated aromatic rings. Finally, this ligand is neutral and so allows for modulation of the architecture of the resulting complexes by the use of linking co-ligands. It is known that the coexistence of different ligands in coordination polymers allows for greater tunability of architectures than a single one, thus providing more versatile CPs. In particular, the combination of neutral and negatively charged

Electronic supplementary material The online version of this article (https://doi.org/10.1007/s11243-019-00323-5) contains supplementary material, which is available to authorized users.

✉ Yun-Shan Xue
yunshanxue1988@163.com

✉ Mei-Pin Liu
liumeipin111@163.com

[1] School of Chemistry and Environmental Engineering, Yancheng Teachers University, Yancheng 224051, Jiangsu, People's Republic of China

[2] School of Chemistry and Bioengineering, Nanjing Normal University Taizhou College, Taizhou 225300, People's Republic of China

[3] National Center of Quality Supervision and Inspection for Tungsten and Rare Earth Products, Ganzhou 341000, Jiangxi, People's Republic of China

ligands can influence the charge density distribution and provide an additional level of control in the resulting structures. A variety of coordination polymers have been prepared by self-assembly from 1,4-bis(benzimidazo-1-ly) benzene with metals including Co, Cd and Zn [15–18]. However, coordination polymers based on 1,4-bis(benzimidazo-1-ly) benzene with polycarboxylic acids as co-ligands are relatively rare [19, 20].

In this study, 1,4-bis(benzimidazo-1-ly) benzene and two different O-donor co-ligands were used based on a dual-ligand strategy, to give two coordination polymers, formulated as $\{[ZnL(mipa)(H_2O)]\}_n$ (**1**) and $\{[Cd_2L_2(sdba)Cl_2]\}_n$ (**2**). Both compounds were characterized by thermogravimetric analyses, elemental analysis, powder X-ray and single-crystal X-ray diffraction. In addition, the photoluminescent properties and photocatalytic activities of the compounds have been investigated.

Experimental section

Materials and methods

All chemicals were commercially available reagent grade and used without further purification. The C, H, N elemental analyses were obtained on a PerkinElmer 240C elemental analyzer. Thermogravimetric analyses (TGA) were conducted on a NETZSCH STA 449 F5 Jupiter TGA analyzer under nitrogen at a heating rate of 10 °C/min. Powder X-ray diffraction (PXRD) patterns were collected on a Shimadzu XRD-6000 X-ray diffractometer using a Cu-Kα radiation ($\lambda = 1.54056$ Å) at room temperature. UV–vis spectra were recorded using a PerkinElmer Lambda 25 spectrophotometer. Photoluminescence (PL) spectra were obtained on a PerkinElmer LS 55 fluorescence spectrophotometer.

Synthesis of compound 1

A mixture of $Zn(NO_3)_2{\cdot}6H_2O$ (0.0148 g, 0.05 mmol), H_2mipa (0.0090 g, 0.05 mmol) and **L** (0.0155 g, 0.05 mmol) in DMF (2 mL) plus H_2O (0.5 mL) was sealed in an autoclave equipped with a Teflon liner (25 mL). The mixture was heated at 110 °C for 3 days and then cooled to room temperature. Yellowish block single crystals of compound **1** were collected in ca. 29% yield based on **L**. Elemental analysis for $C_{32}H_{28}N_4ZnO_5$, calcd (%): C, 62.6; H, 4.6, N, 9.1. Found (%): C, 61.7; H, 4.9, N, 8.5.

Synthesis of compound 2

A mixture of $Cd(NO_3)_2{\cdot}4H_2O$ (0.0155 g, 0.05 mmol), H_2sdba (0.0153 g, 0.05 mmol) and **L** (0.0155 g, 0.05 mmol) in DMF (2 mL), H_2O (1 mL) and 150 µL of HCl (6 mol/L) was sealed in an autoclave equipped with a Teflon liner (25 mL). The mixture was heated at 100 °C for 3 days and then cooled to room temperature. Colorless block single crystals of **2** were collected in ca. 31% yield based on **L**. Elemental analysis for $C_{54}H_{36}Cl_2N_8SCd_2O_6$ calcd (%): C, 53.1; H, 3.0; N, 9.2. Found (%): C, 52.4; H, 3.0; N, 9.0.

Crystal structure determinations

Single-crystal X-ray data collections of both compounds were performed on a Siemens (Bruker) SMART CCD diffractometer using graphite-monochromated Mo-Kα radiation ($\lambda = 0.71073$ Å) at 296 K. The SMART and SAINT software packages were used for data collection and extraction, respectively, and data absorption corrections were performed using the SADABS program [21]. The structures were solved by direct methods and refined on F^2 by full-matrix least-squares methods using the SHELXS program of the SHELXTL package [22]. All the non-hydrogen atoms were refined anisotropically. All H atoms were placed in geometrically calculated positions and refined using the riding model. Details of structural determination and refinement are summarized in Table 1. Selected bond lengths and angles are given in Table 2.

Results and discussion

Synthesis

The two compounds were synthesized solvothermally from the rigid ligand **L** with different co-ligands and metal salts under similar conditions. The two structures are very different. Many factors can influence the structures of such coordination polymers, including the type of metal, counter-anions, pH value and reaction temperature. In this work, we carried out a series of experiments to investigate the effect of the reaction conditions on the crystallinity and identity of the final products. The results indicate that the acid plays an important role in the formation of compound **2** in our reaction system. A small amount of acid could influence the nucleation and/or crystal growth. The absence of the acid resulted in the production of unknown powders. Besides, slight differences in temperature and reagent concentrations have a minor impact on the crystallinity of the resulting products.

Crystal structure of compound 1

Compound **1** crystallizes in a monoclinic *P*21/*c* space group (No. 14) with four asymmetric units per unit cell. The asymmetric unit consists of one zinc atom, one **L**

Table 1 Crystal data and structure refinements for compounds **1**–**2**

Compound reference	**1**	**2**
Chemical formula	$C_{32}H_{28}N_4O_5Zn$	$C_{54}H_{36}Cd_2Cl_2N_8O_6S$
Formula mass	613.97	1220.67
Crystal system	Monoclinic	Monoclinic
a/Å	10.2154(6)	24.5840(13)
b/Å	22.9054(12)	12.5350(6)
c/Å	11.7484(7)	17.3554(9)
α/°	90	90
β/°	96.798(2)	100.2880(10)
γ/°	90	90
Unit cell volume/Å^3	2729.7(3)	5262.3(5)
Temperature/K	173(2)	296.15
Space group	*P*21/*c*	*C*2/*c*
Z	4	4
No. of reflections measured	17,912	17,485
No. of independent reflections	4916	6033
R_{int}	0.0535	0.0303
F(000)	1272	2440
Limits of data collection/°	3.068–25.436	2.101–27.493
μ (mm^{-1})	0.951	1.007
Final R_1 values ($I>2\sigma(I)$)	0.0399	0.0301
Final $wR(F^2)$ values ($I>2\sigma(I)$)	0.0860	0.0701
Final R_1 values (all data)[a]	0.0679	0.0443
Final $wR(F^2)$ values (all data)	0.0932	0.0760
Goodness of fit on F^2	1.050	1.002
CCDC	188,2745	188,2746

[a] $R_1 = \Sigma||F_o| - |F_c||/\Sigma|F_o|$, $wR = [\Sigma w(F_o^2 - F_c^2)^2/\Sigma w(F_o^2)^2]^{1/2}$

Table 2 Selected bond distances (Å) and angles (°) for compounds **1**–**2**

Compound **1**			
Zn1–O1	1.9720(19)	Zn1–O5	1.986(2)
Zn1–O4^i	1.968(2)	Zn1–N1	2.017(2)
O1–Zn1–O5	105.55(8)	O4^i–Zn1–O5	108.74(8)
O1–Zn1–N1	116.71(9)	O4^i–Zn1–N1	106.98(9)
O4^i–Zn1–O1	102.66(8)	O5–Zn1–N1	115.29(9)
Compound **2**			
Cd1–Cl1	2.5854(7)	Cd1–O1	2.2940(18)
Cd1–Cl1^i	2.6014(7)	Cd1–O2	2.4155(18)
Cd1–N1	2.3820(19)	Cd1–N4^{ii}	2.3559(19)
Cl1–Cd1–Cl1^i	93.79(2)	N1–Cd1–Cl1	92.70(5)
O1–Cd1–Cl1	156.91(6)	N1–Cd1–Cl1^i	95.22(5)
O1–Cd1–Cl1^i	109.26(5)	N1–Cd1–O2	83.46(7)
O1–Cd1–O2	55.80(7)	N1–Cd1–C1	84.36(8)
O1–Cd1–N1	86.60(7)	N4^{ii}–Cd1–Cl1	91.28(5)
O1–Cd1–N4^{ii}	88.54(7)	N4^{ii}–Cd1–Cl1^i	87.57(5)
O2–Cd1–Cl1	101.17(5)	N4^{ii}–Cd1–O2	92.76(7)
O2–Cd1–Cl1^i	165.02(5)	N4^{ii}–Cd1–N1	174.98(7)

Symmetry transformations: for **1** (i) $x+1$, y, z; (ii) $x-1$, y, z; for **2** (i) $2.5-x$, $0.5-y$, $-z$; (ii) $0.5+x$, $0.5+y$, z; (iii) $2-x$, y, $0.5-z$; (iv) $-0.5+x$, $-0.5+y$, z

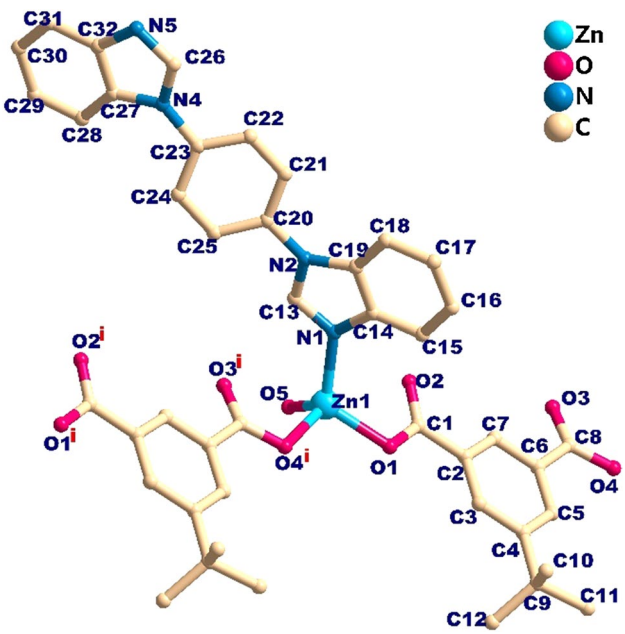

Fig. 1 Coordination environment of Zn center in compound **1**

ligand, one fully deprotonated H_2mipa ligand and one coordinated water ligand. As shown in Fig. 1, each Zn center is tetra-coordinated by one nitrogen atom from an **L** ligand (Zn1–N1 = 2.017(2) Å), two oxygen atoms from two crystallographically equivalent mipa^{2-} ligands (Zn1–O1 = 1.9720(19) Å; Zn1–O4 = 1.968(2) Å) and one oxygen from the water ligand (Zn1–O5 = 1.986(2) Å), forming a tetrahedral coordination geometry. The bond distances are comparable to those reported for similar zinc complexes [19].

Each fully deprotonated mipa^{2-} ligand, in a "V-shaped" conformation, connects two Zn atoms by a monodentate mode to construct a 1D infinite $[Zn(mipa)]_n$ chain, while the **L** and water ligands occupy the remaining coordination sites, with an adjacent Zn···Zn distance of 10.215 Å (Fig. 2a). The **L** ligand is neutral, and its two benzimidazole rings are coplanar, with a dihedral angle of 0°. The dihedral angle between the benzene ring (C20–C21–C22–C23–C24–C25) and the benzimidazole ring (C14–C15–C16–C17–C18–C19–N2–C13–N1) is 33.42°. The benzimidazole rings of **L** within the chains are parallel to each other, with an interplanar distance of 5.056 Å.

The 1D chains of compound **l** are linked by hydrogen bonds (O–H···N = 2.688(3) Å) between the water ligands and the N atoms of the benzimidazole rings of **L,** forming

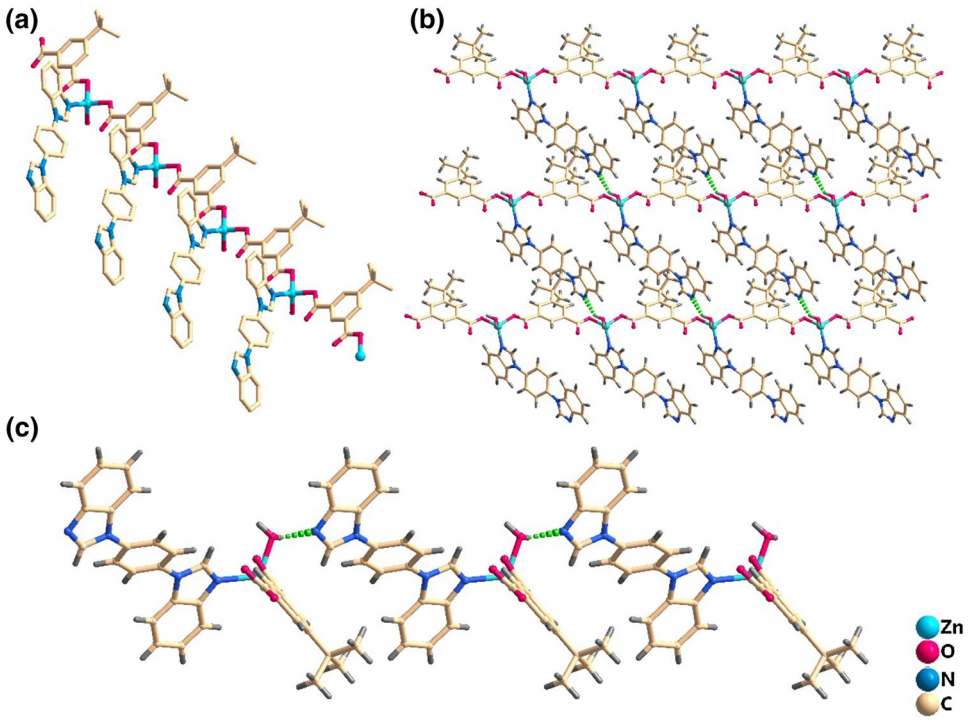

Fig. 2 **a** A drawing showing 1D chain; **b**, **c** a drawing showing the 2D layer oriented stacked by H-bonding interactions along ***b*** and ***a*** axis, respectively

a 2D layer along the ***b*** axis (Fig. 2b). Adjacent 2D layers are further connected into a 3D supramolecular structure through $\pi\cdots\pi$ interactions [Cg1–Cg2 = 3.7532(19) Å, Cg2–Cg2 = 3.8199(19) Å, Cg2–Cg6 = 3.612(2) Å, Cg4–Cg6 = 3.675(2) Å, Cg5–Cg5 = 3.997(17) Å] between the phenyl and benzimidazole rings, which help to stabilize the 3D network (Fig. 3) [23]. The sheets are stacked over each other in an ABCD manner along the ***c***-axis (Fig. 4a). The 3D supramolecular structure and the stacking architecture are illustrated in Fig. 4 and S3.

To further understand the architecture of compound **1**, topological analysis was performed with the TOPOS programs [24]. The Zn centers can be simplified as 4-connected nodes, while the H_2mipa and **L** ligands are considered as simple linkers. Hence, the 2D layer structure through hydrogen bonds can be simplified as a 4-connected ***sql*** net with point symbol of $\{4^4.6^2\}$ (Fig. 4b).

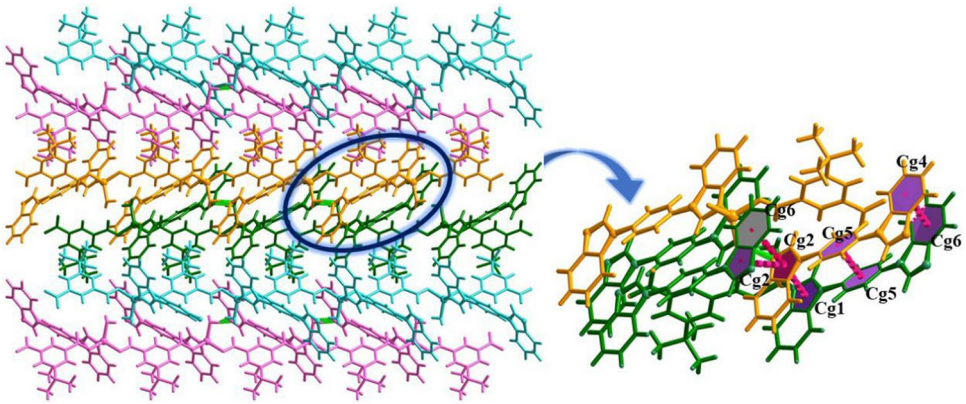

Fig. 3 3D supramolecular structure of compound **1** constructed by $\pi\cdots\pi$ interactions viewed along the ***c***-axis. The inset exhibits the details of $\pi\cdots\pi$ interactions (shown as red dotted line; Cg1 is the centroid of the ring that is composed of N1, C13, N2, C19 and C14; Cg2 is the centroid of the ring that is composed of N4, C26, N5, C32 and C27; Cg4 is the centroid of the ring which contains C14, C15, C16, C17, C18 and C19; Cg5 is the centroid of the ring which contains C20, C21, C22, C23, C24 and C25; Cg6 is the centroid of the ring which is composed of C27, C28, C29, C30, C31 and C32)

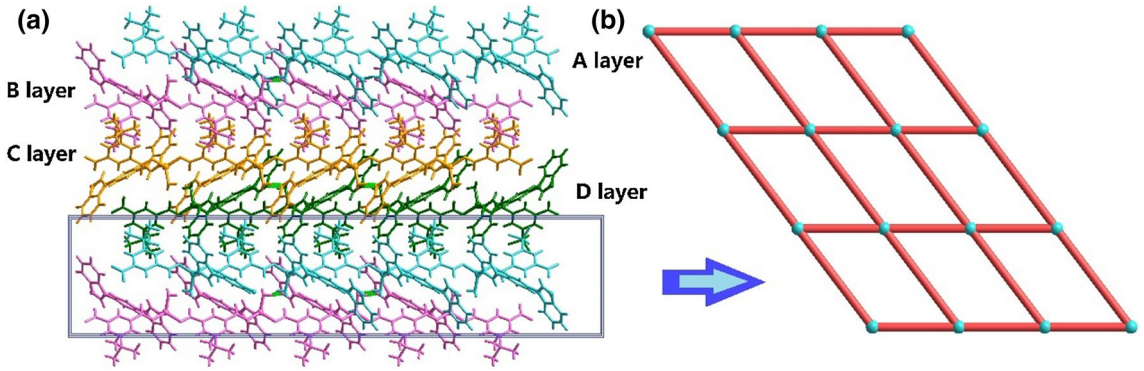

Fig. 4 **a** 3D supramolecular structure of **1** and the stacking manner along ***c***-axis; **b** the 2D layer formed by hydrogen bonds with ***sql*** topology

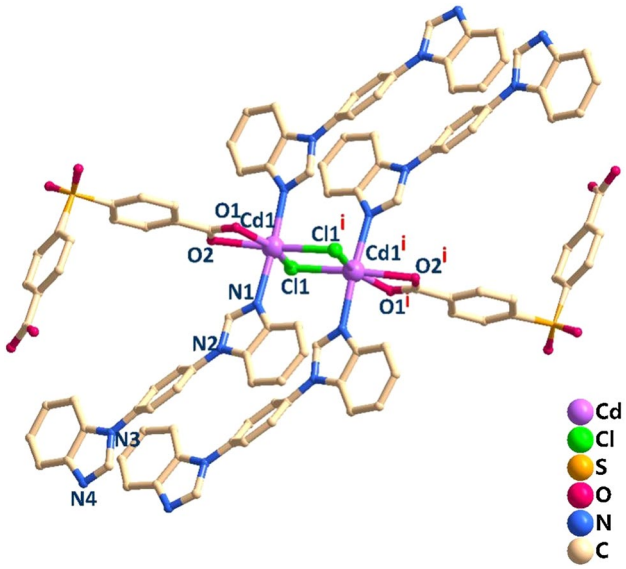

Fig. 5 Coordination environment of Cd atoms in compound **2**

Crystal structure of compound 2

Compound **2** crystallizes in the monoclinic space group *C*2/*c* with four asymmetric units in each cell. The asymmetric unit contains one crystallographically independent cadmium atom, one chlorine atom, one **L** ligand and half of a fully deprotonated H_2sdba ligand. As depicted in Fig. 5, the Cd atom is six-coordinated by two O atoms from one chelating bidentate carboxylate group of an $sdba^{2-}$ ligand, two N atoms provided by two **L** ligands and two Cl atoms, giving a slightly distorted octahedral geometry. The equatorial plane is occupied by atoms O1 and O2 from the $sdba^{2-}$ ligand and two Cl atoms, while the axial sites are occupied by two N atoms from **L** ligands. The *X*–Cd–*X* angles (where *X* is a basal N or O atom) range from 55.80(7) to 174.98(7) ° and the octahedron edge lengths range from 2.2062(26) to 3.9959(21). The Cd–O and Cd–N bond lengths are in the ranges of 2.2940(18) to 2.4155(18) Å and 2.3559(19) to 2.3820(19) Å, respectively.

Neighboring Cd centers (Cd1 and symmetry-related Cd1A) are linked together by two –Cl– bridges to form a dinuclear $[Cd_2(COOR)_2N_2Cl_2]$ SBU, with the Cd···Cd distance equal to 3.5444(6) Å. Each SBU connects four **L** ligands and two fully deprotonated $sdba^{2-}$ ligands. The two benzimidazole rings of the **L** ligands are coplanar; each SBU connects four **L** ligands which are parallel to each other. The **L** ligand adopts an "*I*-shape" conformation to connect two neighboring SBUs to into a 1D ladder chain (Fig. 6a). The $sdba^{2-}$ ligand has an approximately "L-shape" geometry and bridges neighboring SBUs to form a linear zigzag chain along the ***a*** direction (Fig. 6b, c). These 1D ladder chains are extended into a 3D network by connecting with the SBUs and $sdba^{2-}$ ligands, as illustrated in Fig. 6d. In addition, other $[Cd_2(COOR)_2N_2Cl_2]$ SBUs are oriented perpendicular to those in the 1D ladder chains, being linked by four **L** ligands to form an independent unit (Fig. 6e). These units are integrated into the above-mentioned 3D network, resulting in a novel and complicated 3D structure (Fig. 6f).

Structural comparisons

Comparing the structures of the two compounds, the ligand **L** adopts the same coordination mode acting simply as a linker, whereas the different coordination modes and geometries of the co-ligands determine the final structures. In compound **1**, each Zn atom is coordinated by two monodentate carboxylate groups of different $mipa^{2-}$ ligands, while the two remaining coordination sites are occupied by **L** and water ligands. Two carboxylate groups of the $mipa^{2-}$ ligand coordinate two Zn atoms to give 1D chains, which are further extended to a 2D structure by hydrogen bonds. Only 4-connected nodes are present in the 2D network, which can be simplified as a 4-connected ***sql*** topology. Adjacent layers are further stacked into a 3D supramolecular structure by $\pi\cdots\pi$ interactions. In compound **2**, two Cl^- anions

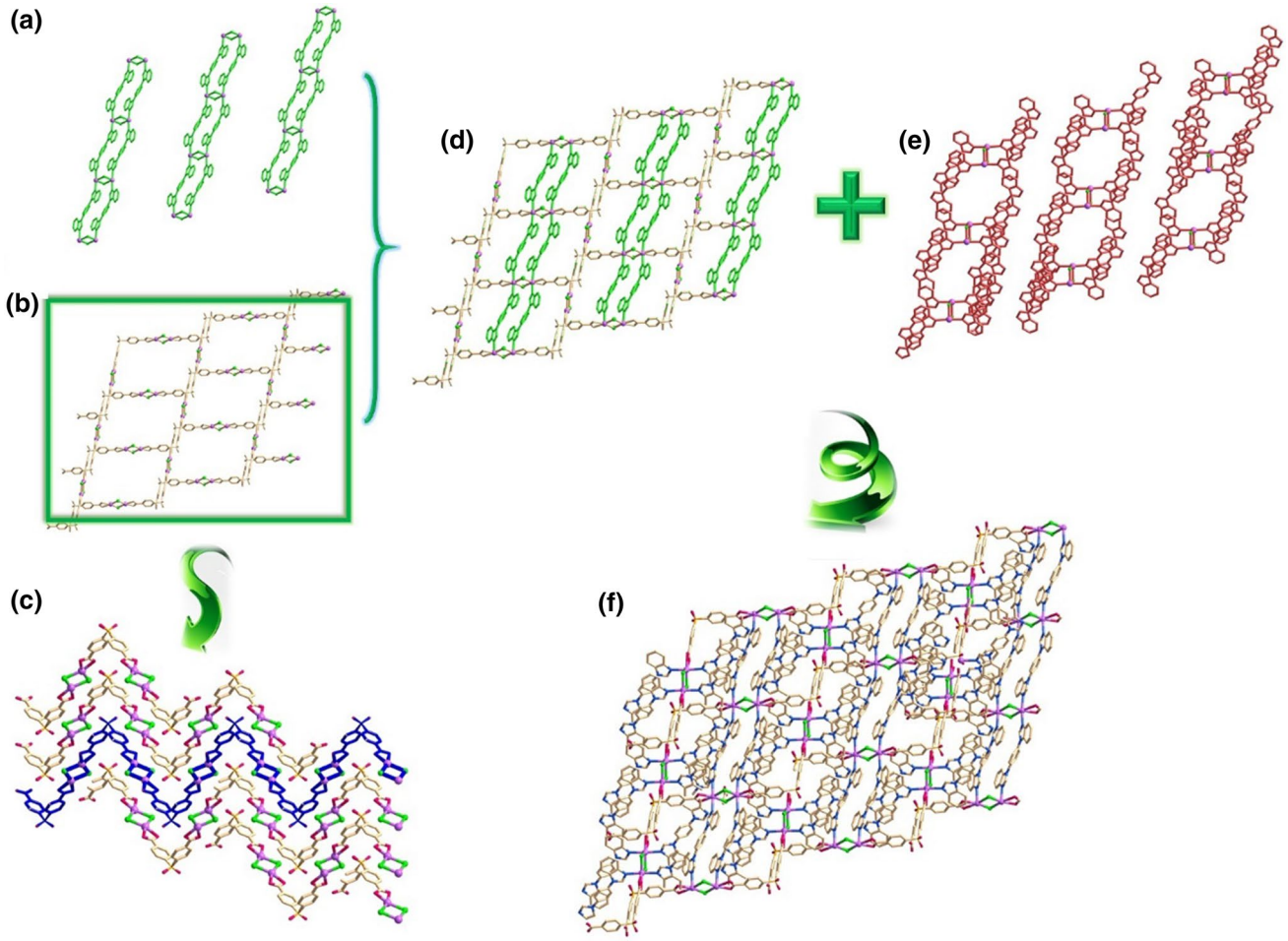

Fig. 6 **a** 1D ladder chains formed by dinuclear $[Cd_2(COOR)_2N_2Cl_2]$ SBUs and **L** ligands; **b**, **c** 1D zigzag chains formed by $[Cd_2(COOR)_2N_2Cl_2]$ SBUs and ∟-shaped ligands $sdba^{2-}$ along ***a*** direction; **d** 1D ladder chains are extended to a 3D network structure; **e** other kind of $[Cd_2(COOR)_2N_2Cl_2]$ SBUs oriented perpendicular; **f** 3D complicated structure of compound **2**

bridge neighboring Cd atoms into a dinuclear cluster, which connects with four **L** and two $sdba^{2-}$ ligands to obtain an intricate 3D architecture.

Thermogravimetric analysis

The thermal stabilities of these compounds were investigated using single-crystal samples under N_2 atmosphere. As shown in Fig. 7, compound **1** exhibited a weight loss of 2.7% at 25–145 °C, attributed to the loss of coordinated water (calcd 2.9%). Upon further heating, compound **1** remained stable up to 270 °C. After that temperature, the compound decomposed with an abrupt weight loss. The final mass remnant corresponds to ZnO (calculated 13.2%, observed 10.2%). For compound **2**, the framework remained stable up to 260 °C. The TGA curve then showed an abrupt weight loss of 38.4% between 260 and 320 °C (calculated 38.6%) corresponding to the loss of ligand $sdba^{2-}$ and Cl^- anions. A further weight loss between 335 and 550 °C may be ascribed to the decomposition of the ligand **L** (calculated 50.8%, observed 52.0%). The remaining weight of 7.3% corresponds to a likely formation of CdO (calculated 10.5%).

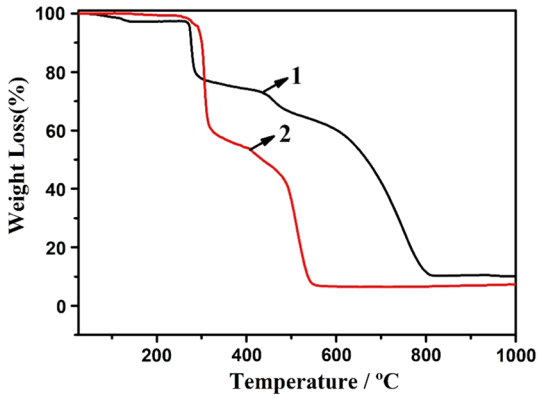

Fig. 7 TGA curves for compounds **1**–**2**

Photoluminescent properties

The solid-state photoluminescence spectra of both compounds were recorded at room temperature. As shown in Figure S4, the free ligands **L**, H_2mipa, and H_2sdba exhibit maxima at 422 (λ_{ex} = 343 nm), 328 (λ_{ex} = 280 nm) and 350 nm (λ_{ex} = 310 nm), respectively, which can be assigned to $\pi^* \rightarrow \pi$ or $\pi^* \rightarrow$ n transitions [25, 26]. Compounds **1** and **2** show blue fluorescence emission peaks at 362 nm (λ_{ex} = 320 nm) and 356 nm (λ_{ex} = 306 nm), respectively (Figure S5 and S6). Since Zn(II) and Cd(II) are difficult to oxidize or reduce owing to their d^{10} electronic configurations, the emission bands of compounds **1** and **2** are not likely to arise from ligand-to-metal charge transfer (LMCT) or metal-to-ligand charge transfer (MLCT). Hence, these emissions are most probably derived from intraligand and/or ligand-to-ligand charge transfer (LLCT) transitions [27, 28].

Heavy metals such as Hg(II), Cr(III) and Cd(II) are common contaminants in industrial wastewater, which are easily accumulated in living organisms. To explore the sensing ability of compounds **1** and **2**, experiments were performed on aqueous solutions of various metal ions. However, compound **1** is soluble in water if left for sufficient time. Therefore, only compound **2** was selected for investigation as a potential sensor material. Finely ground samples of **2** were dispersed in aqueous solutions of different $M(NO_3)_x$ salts (2 mL, 0.01 mol L^{-1}) for fluorescence measurements (M = Ca^{2+}, Mg^{2+}, Cu^{2+}, Ni^{2+}, Co^{2+}, Zn^{2+}, Cd^{2+}, Hg^{2+}, K^+, Ag^+, Al^{3+}, Fe^{3+}, Cr^{3+}). The emission intensities of compound **2** were found to vary with metal ions. As shown in Fig. 8, the fluorescence intensity was significantly quenched by Hg^{2+} compared to several other metal ions (Ca^{2+}, Mg^{2+}, Ni^{2+}, Co^{2+}, Zn^{2+}, K^+, Ag^+), while Cu^{2+}, Cd^{2+}, Al^{3+}, Fe^{3+} and Cr^{3+} revealed partial quenching behavior. To further explore the sensitivity of **2** toward Hg^{2+}, different concentrations of $Hg(NO_3)_2$ (10^{-6}–10^{-1} mol/L) were investigated in fluorescence experiments in aqueous solution. As shown in Fig. 9, the emission intensity of **2** gradually decreased with increasing concentrations of Hg^{2+}, such that the quenching efficiency reached 95% when the concentration of Hg^{2+} was to 10^{-1} mol/L (Fig. 10).

The quenching efficiency was calculated from the equation $(I_0 - I)/I_0 \times 100\%$, where I_0 and I represent the fluorescence intensity of compound **2** before and after the addition of Hg^{2+}, respectively. A plot of fluorescence intensity against Hg^{2+} concentration in the low concentration range of 0–10^{-3} mol/L was analyzed with the Stern–Volmer equation, $I_0/I = K_{SV}[Hg^{2+}] + 1$ (where K_{SV} is the quenching constant). The Stem–Volmer plot reveals a good linear correlation at low concentrations, which could be fitted as $I_0/I = K_{SV}[Hg^{2+}] + 1.14$, with a quenching constant of 6.07×10^3 L/mol (Fig. 11).

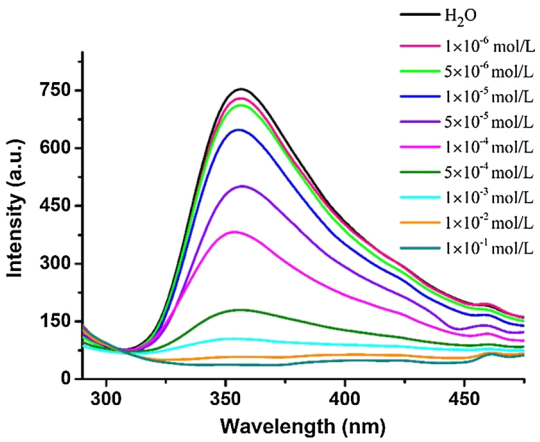

Fig. 9 Emission spectra of **2** dispersed in aqueous with different concentrations of Hg^{2+} (λ_{ex} = 306 nm)

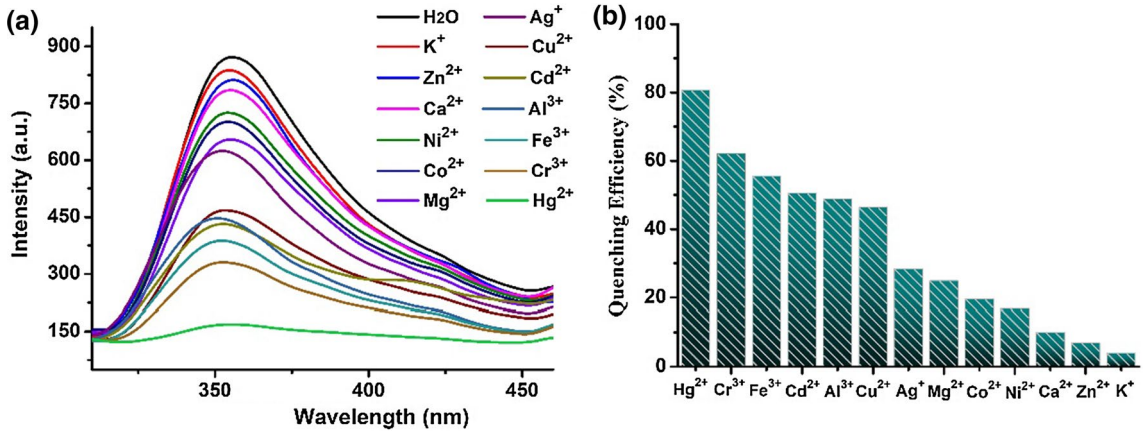

Fig. 8 **a** Photoluminescent spectra for compound **2** after the samples were dispersed in 10^{-2} mol/L concentration of aqueous solutions containing different metal ions; **b** quenching efficiency histogram of **2**

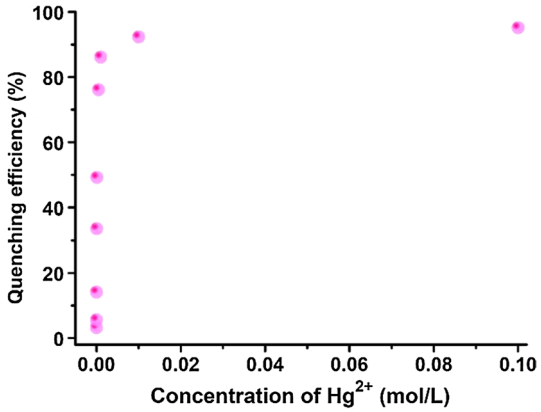

Fig. 10 Dependence of the quenching efficiency on the concentration of Hg^{2+}

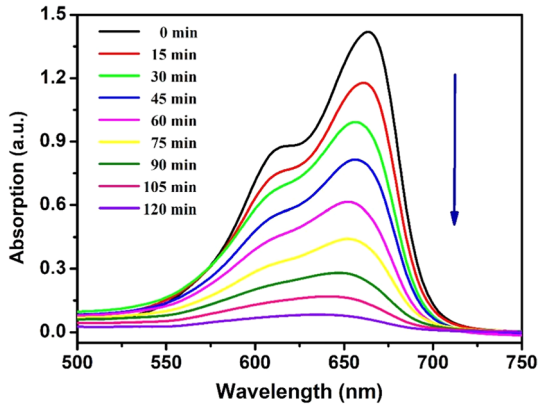

Fig. 12 Absorption spectra of the MB solution under UV irradiation in the presence of compound **2**

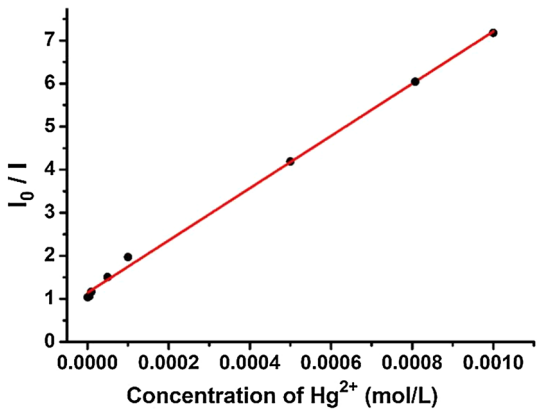

Fig. 11 Stern–Volmer plot of **2** with different concentrations of Hg^{2+}

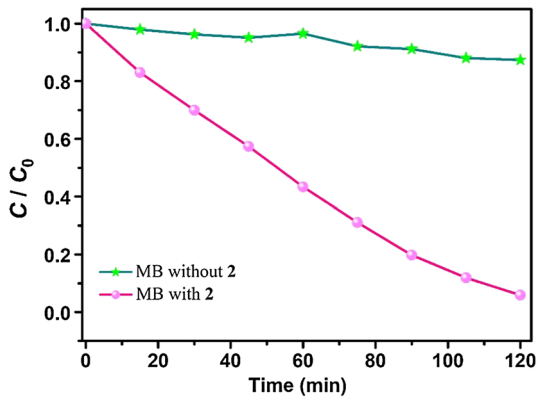

Fig. 13 Plot of concentration ratios (c/c_0) against irradiation time (min) of MB

Photocatalytic degradation of organic dyes

The release of industrial wastewater containing organic dyes into the environment is a source of environmental problems, since organic dyes are usually toxic and even carcinogenic. A number of papers have suggested that d^{10} metal complexes can show excellent photocatalytic performance for the degradation of organic dyes under UV irradiation [29–33]. Hence, in order to investigate the photocatalytic activity of compound **2**, four common organic dyes, namely rhodamine B (RhB), methylene blue (MB), methyl orange (MO) and malachite green oxalate (MGO), were selected for degradation experiments. The results of these experiments show that compound **2** is ineffective for degrading MO, RhB and MGO. Hence, we performed further photocatalytic experiments for degradation of MB only. The photocatalytic reactions were carried out in aqueous solution with UV irradiation in a typical process as follows. A sample of compound **2** (30 mg) was dispersed in 50 mL of aqueous MB solution and stirred in the dark for 30 min to establish an adsorption/desorption equilibrium. The mixture was then placed under UV irradiation from a 300 W Hg lamp and stirred constantly. Aliquots of the mixture were removed at 15 min intervals and analyzed by UV–vis spectroscopy. As depicted in Fig. 12, the maximum absorbance intensity of MB decreased obviously with increasing reaction time in the presence of **2** as a photocatalyst, such that the dye was almost completely degraded after 120 min. As illustrated in Fig. 13, a blank experiment was conducted for MB in the absence of the photocatalyst, whereupon the degradation efficiency was reduced to 12.7%.

These results indicate that compound **2** has photocatalytic activity for the degradation of MB in water. The degradation kinetics were evaluated by a first-order kinetic model [34]:

$$\ln\left(C_0/C\right) = kt \quad (1)$$

where the slope k is the apparent reaction rate constant and C_0 and C represent the initial concentration of dye and the concentration at reaction time t, respectively. As shown in

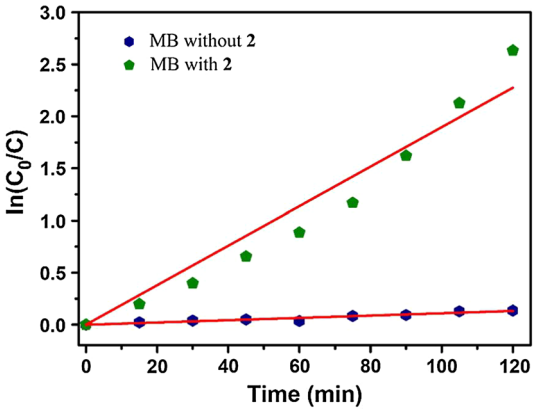

Fig. 14 Photocatalytic degradation kinetics of **2** for organic dye MB using first-order kinetic model

Fig. 14, the degradation plots gave a good fit to the first-order kinetic function. The calculated apparent rate constant k is 0.019 min^{-1} in the presence of **2**, while the rate constant was 0.0011 min^{-1} for the blank experiment.

The possible photocatalytic mechanism can be proposed based on related studies [35, 36]. Under UV–vis light, the organic ligand L and carboxylate ligand may be excited to generate N–Cd and/or O–Cd charge transfer, promoting the formation of electron–hole pairs. These photo-generated holes react with water to give hydroxyl radicals, which can effectively decompose dyes to complete the photocatalytic process [37, 38]. Moreover, the conduction band electrons can be captured by dissolved O_2 to form the superoxide radical $\cdot O_2^-$, which can be converted to ·OH radicals through combination with H^+ from water.

Conclusion

In summary, two novel coordination polymers based on 1,4-bis(benzimidazo-1-ly)benzene (**L**) and O-donor co-ligands have been solvothermally synthesized and characterized. Compound **1** has a 3D supramolecular structure supported by hydrogen bonds and π–π interactions. Compound **2** is constructed from dinuclear $[Cd_2L_4Cl_2]$ SBUs and V-shaped $sdba^{2-}$ linkers, forming a complicated 3D architecture. Both compounds are photoluminescent at room temperature, and the emission of **2** can be quenched efficiently by Hg(II) ion. Moreover, compound **2** acts as a photocatalyst for degradation of methylene blue under UV irradiation. The preparations of these compounds demonstrate that the dual-ligand strategy is useful for the construction of coordination polymers with interesting structures and properties.

Supplementary material

CCDC 1882745 (**1**), 1882746 (**2**) contain the supplementary crystallographic data for this paper. These data can be obtained free of charge from The Cambridge Crystallographic Data Centre via www.ccdc.cam.ac.uk/data_request/cif.

Acknowledgements This work was supported by the National Natural Science Foundation of China (Grant No. 21501147), the Natural Science Foundation of Jiangsu Province (Grant No. BK20160442), University Science Research Surface Project of Jiangsu Province (Grant No. 16KJB150039) and A Project Funded by the Excellent Specialties Program Development of Jiangsu Higher Education Institutions (Grant No. PPZY2015B113).

References

1. Vellingiri K, Philip L, Kim KH (2017) Coord Chem Rev 353:159–179
2. Park HD, Dinca M, Roman-Leshkov Y (2018) J Am Chem Soc 140:10669–10672
3. Dong XW, Yang Y, Che JX, Zuo J, Li XH, Gao L, Hu YZ, Liu XY (2018) Green Chem 20:4085–4093
4. Zhang J, Huang Y, Yue D, Cui Y, Yang Y, Qian G (2018) J Mater Chem B 6:5174–5180
5. Jiang M, Li P, Wu P, Zhang F, Tian X, Deng C, Wang J (2018) Chem Commun 54:9131–9134
6. Sun X, Yao S, Yu C, Li G, Liu C, Huo Q, Liu Y (2018) J Mater Chem A 6:6363–6369
7. Zhang M, Zhou W, Pham T, Forrest KA, Liu W, He Y, Wu H, Yildirim T, Chen B, Space B (2017) Angew Chem Int Ed 56:11426–11430
8. Alezi D, Belmabkhout Y, Suyetin M, Bhatt PM, Weselinski LJ, Solovyeva V, Adil K, Spanopoulos L, Trikalitis PN, Emwas AH (2015) J Am Chem Soc 137:13308–13318
9. Prasetya N, Donose BC, Ladewig BP (2018) J Mater Chem A 6:16390–16402
10. Meng X, Zhang X, Bing Y, Xu N, Shi W, Cheng P (2016) Inorg Chem 55:12938–12943
11. Han J, Wang D, Du YH, Xi S, Hong J, Yin S, Chen Z, Zhou T, Xu R (2015) J Mater Chem A 3:20607–20613
12. Li M, Zhao S, Peng YF, Li BL, Li HY (2013) Dalton Trans 42:9771–9776
13. Hao JM, Yu BY, Van Hecke K, Cui GH (2015) CrystEngComm 17:2279–2284
14. Zhu X, Zhao S, Peng YF, Li BL, Wu B (2013) CrystEngComm 15:9154–9159
15. Li CY, Li L, Hu TL (2011) J Inorg Organomet Polym 21:682–687
16. Li L, Hu TL, Zeng YF, Bu XH (2010) Sci China Chem 53:2170–2176
17. Li ZX, Xu Y, Zuo Y, Li L, Pan Q, Hu TL, Bu XH (2009) Cryst Growth Des 9:3904–3909
18. Li ZX, Hu TL, Ma H, Zeng YF, Li CJ, Tong ML, Bu XH (2010) Cryst Growth Des 9:1138–1144
19. Wu MK, Yi FY, Fang Y, Xiao XW, Wang SC, Pan LQ, Zhu SR, Tao K, Han L (2017) Cryst Growth Des 17:5458–5464
20. Hu T, Wang X, Xue Z, Zhang X, Wang X (2017) Polyhedron 127:449–457
21. SMART and SADABS (1997) Bruker AXS Inc., Madison

22. Sheldrick GM (2015) Acta Crystallogr Sect C 71:3–8
23. Hu T, Wang X, Xue Z, Zhang X, Wang X (2017) Polyhedron 127:449–457
24. Blatov VA (2004) TOPOS, A multipurpose crystallochemical analysis with the program package. Samara State University, Samara
25. Lakowicz JR (2006) Principles of fluorescence spectroscopy, 3rd edn. Springer, Berlin
26. Valeur B (2002) Molecular fluorescence: principles and application. Wiley-VCH, Weinheim
27. Ma LF, Wang LY, Hu JL, Wang YY, Yang GP (2009) Cryst Growth Des 9:5334–5342
28. Sun D, Yan ZH, Blatov VA, Wang L, Sun DF (2013) Cryst Growth Des 13:1277–1289
29. Liu L, Ding J, Huang C, Li M, Hou H, Fan Y (2014) Cryst Growth Des 14:3035–3041
30. Hao J, Yu B, Van Hecke K, Cui G (2015) CrystEngComm 17:2279–2293
31. Kan WQ, Liu B, Yang J, Liu YY, Ma JF (2012) Cryst Growth Des 12:2288–2298
32. Das MC, Xu H, Wang Z, Srinivas G, Zhou W, Yue YF, Nesterov VN, Qian GD, Chen B (2011) Chem Commun 47:11715–11717
33. Zhang T, Lin W (2014) Chem Soc Rev 43:5982–5993
34. Ramasundaram S, Seid MG, Choe JW, Kim EJ, Chung YC, Cho K, Lee C, Hong SW (2016) Chem Eng J 306:344–349
35. Wu XY, Qi HX, Ning JJ, Wang JF, Ren ZG, Lang JP (2015) Appl Catal B 168:98–104
36. Liu J, Xiao J, Wang D, Sun W, Gao X, Yu H, Liu H, Liu Z (2017) Cryst Growth Des 17:1096–1102
37. Yang HX, Liu TF, Cao MN, Li HF, Gao SY, Cao R (2010) Chem Commun 46:2429–2431
38. Meng XM, Fan CB, Bi CF, Zong ZA, Zhang X, Fan YH (2016) CrystEngComm 18:2901–2912

Publisher's Note Springer Nature remains neutral with regard to jurisdictional claims in published maps and institutional affiliations.